AETHER
Atmospheric Electrochemical Transformation for Habitat and Environmental Regeneration
2026 Human Lander Challenge Proposal
Embry-Riddle Aeronautical University

Grant Bowers Undergraduate Sr. Software Eng. Program Manager	**Sanaya Nichani** Undergraduate Jr. Aerospace Eng. Dep. Program Manager	**David Clay** Undergraduate Sr. Aerospace Eng. Technology Officer	**Max Klein** Undergraduate Soph. Aerospace Eng. Safety Officer
Cooper Nelson Undergraduate Soph. Aerospace Eng. Testing Officer	**Trinidy Boyce** Undergraduate Jr. Aerospace Eng.	**Lucas Cooper** Undergraduate Soph. Aerospace Eng.	**Maleah Davis** Undergraduate Fresh. Aerospace Eng.
Caleb Del Rosario Undergraduate Fresh. Aerospace Eng.	**R. Jacob Labagh** Undergraduate Fresh. Aerospace Eng.	**Christopher LeClair** Undergraduate Soph. Aerospace Eng.	**Bergen Lien** Undergraduate Fresh. Mechanical Eng.
Leah Little Undergraduate Fresh. Mechanical Eng.	**Cambri Miller** Undergraduate Sr. Aerospace Eng.	**Isabel Scalia** Undergraduate Fresh. Aerospace Eng.	**Kira Schroeder** Undergraduate Fresh. Aerospace Eng.
Owen Smith Undergraduate Jr. Mechanical Eng.	**Samyukta Sudheer** Undergraduate Jr. Aerospace Eng.	**Dr. Siwei Fan** Academic Mentor Aerospace Eng.	**Dr. Ron Madler** Academic Mentor Aerospace Eng.

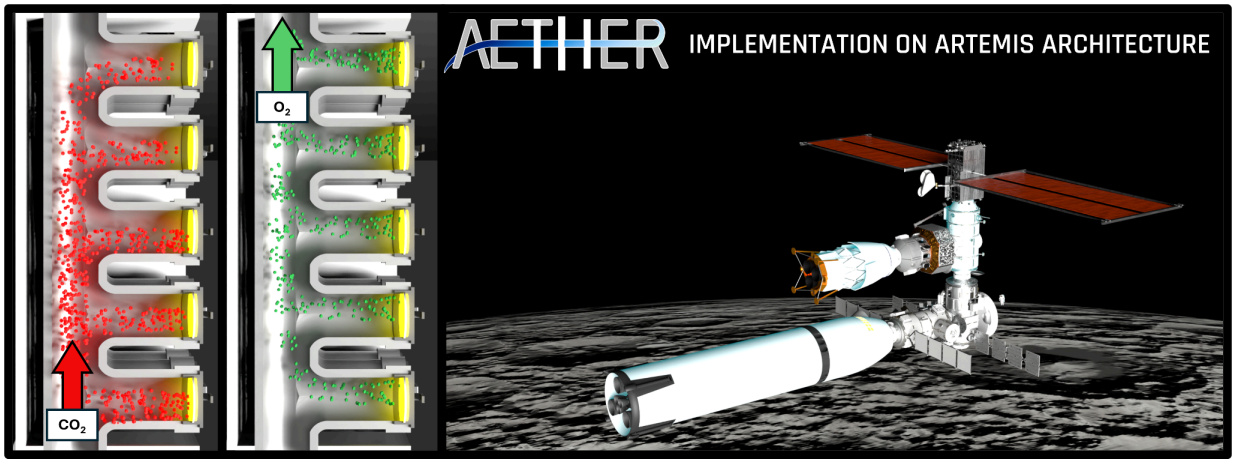

To the HuLC Project Lead: I, Siwei Fan , hereby attest that I have reviewed and approved the proposal submission for the project, titled, **AETHER**, Atmospheric Electrochemical Transformation for Habitat and Environmental Regeneration, from, Embry-Riddle Aeronautical University,

(signature)

May-27-2026
(date)

Table of Contents

Table of Figures

Table of Tables

Table of Acronyms

Acronym	Definition
AETHER	Atmospheric Electrochemical Transformation for Habitat and Environmental Regeneration
CDRA	Carbon Dioxide Removal Assembly
CER	Cost Estimating Relationship
CRS	Carbon Dioxide Reduction System
ECLSS	Environmental Control and Life Support Systems
FPC	First Pound Cost
HLS	Human Lander System
HuLC	Human Lander Challenge
ISS	International Space Station
kg/cm-d	Kilograms per Crew Member per Day
LEO	Low Earth Orbit
LiTFSI	Lithium bis(trifluoromethanesulfonyl)imide
MOOSE	Multiphysics Object-Oriented Simulation Environment
NASA	National Aeronautics and Space Administration
OGA	Oxygen Generation Assembly
OGS	Oxygen Generation System
P2D	Pseudo-2D
PARSEC	Professional Association of Research for Space Engineering Concepts
PBM	Planetary Ball Mill
PCEC	Project Cost Estimating Capability
PDEs	Partial Differential Equations
PEEK	Polyether ether ketone
PTFE	Polytetrafluoroethylene
PVC	Polyvinyl Chloride
TEGDME	Tetraethylene glycol dimethyl ether
TRL	Technology Readiness Level
USD	United States Dollar
WRS	Water Recovery System

Quad Chart

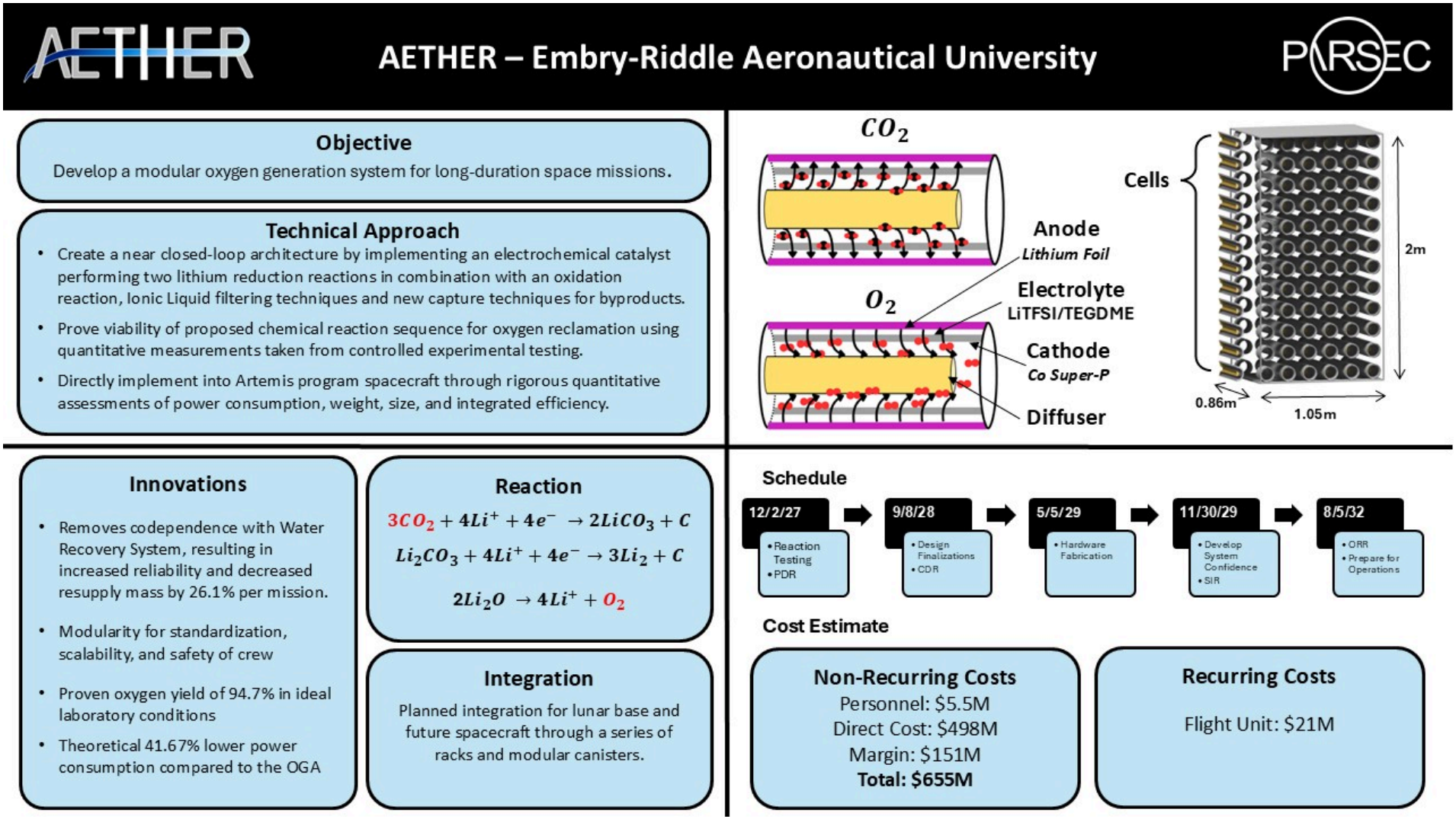

Figure 1: Quad Chart

Technical Paper

1.1. Executive Summary

Current oxygen reclamation systems aboard the International Space Station (ISS) and other spacecraft are unable to meet sustainability requirements for future long-term lunar and Martian missions [1]. Future systems must resolve current capability gaps, specifically reliance on initial reserve supply or resupply. The Professional Association of Research for Space Engineering Concepts (PARSEC) proposes Atmospheric Electrochemical Transformation for Habitat and Environmental Regeneration (AETHER): a system that separates CO_2 to produce O_2 via three electrochemical reactions occurring at room temperature. AETHER improves upon existing flight-proven oxygen reclamation systems in five primary areas: increased reclamation efficiency, decreased mass requirement, decreased system complexity, decreased power consumption, and increased modularity.

1.2. Problem Statement

The effectiveness of human space exploration for 30-day lunar surface and 1200-day martian missions are contingent on the ability of Environmental Control and Life Support Systems (ECLSS) to operate with limited, or nonexistent, resupply and repair [2]. Efficiency of oxygen recovery from crew-generated CO_2 is a limiting factor that creates interdependency between recovery hardware and consumable resupply. Current architecture on the International Space Station (ISS) regulates CO_2 and O_2 via the CO_2 Reduction System (CRS), Oxygen Generation Assembly (OGA) and Sabatier reaction. The OGA performs solid polymer electrolysis on water provided by the Water Recovery System (WRS), resupply, and the Sabatier reaction [3] [4]. The Sabatier reaction creates water from hydrogen byproducts during electrolysis of water in the OGA [5]. Current ECLSS methods can achieve a sustained O_2 reclamation efficiency of 51%, yet National Aeronautics and Space Administration (NASA) sources claim long-term Mars or lunar operations require an oxygen recovery target greater than 75% [1] [6].

A current alternative to achieve greater O_2 recovery yield is the Series-Bosch system, which can achieve a theoretical efficiency of 100% O_2 recovery [7]. However, the Series-Bosch system presents inherent risks and integration issues into spacecraft [8]. When implemented, the Series-Bosch would require hydrogen to be taken from the OGA to split CO_2, creating the need for either pre-existing OGA or additional hydrogen storage. Additionally, the Series-Bosch operates at 500-650 °C, which leads to increased power consumption and complex thermal control loop requirements to bring the system's factor of safety within acceptable ranges [9]. Because the Series-Bosch requires additional hydrogen storage, OGA augmentation, and thermal control loops, ECLSS complexity rises dramatically [8]. For long-term Human Lander System (HLS), lunar base, or Mars missions, current oxygen reclamation systems would be insufficient or infeasible for implementation without major redesign to multiple existing ECLSS subsystems.

1.3. Solution

To improve oxygen reclamation processes for future long-duration missions, the Professional Association of Research for Space Engineering Concepts (PARSEC) proposes Atmospheric Electrochemical Transformation for Habitat and Environmental Regeneration (AETHER), a system that utilizes three electrochemical reactions, between a Co-Super P carbon cathode and a Li metal anode, that reclaims O_2 from CO_2 through operating at varying voltages. AETHER operates as a series of modular electrochemical canisters, called cells, this process can occur at varying rates in order to support crews of different sizes and in locations both on and off spacecraft. AETHER has been designed to operate at room temperature, converting pre-collected CO_2 from existing ECLSS scrubbing systems with a theoretical 94.7% yield [10]. In addition, AETHER can operate under varying atmospheric concentrations provided CO_2 is present, rather than requiring a pure CO_2 input, thus allowing the conversion of Martian

atmospheric CO_2 into oxygen. Unlike existing ECLSS systems on the ISS, AETHER does not require water to operate. Thus, analysis has shown a significant reduction in operational and resupply costs due to AETHER eliminating the need to recycle hydrogen and methane byproducts.

1.4. Innovation

Existing oxygen reclamation architectures, particularly the Series-Bosch Reactor and the Oxygen Generation System (OGS) aboard the ISS, exhibit clear drawbacks that limit implementation on long-duration crewed spaceflights. For instance, the Series-Bosch operates at extreme temperatures, heavy power draw, and high system complexity [8]. Though flight-proven, the OGS requires resupply of water, performs with a low 51% reclamation efficiency, and depends on other systems' functionality, such as the Sabatier, to produce a consistent supply of oxygen [11].

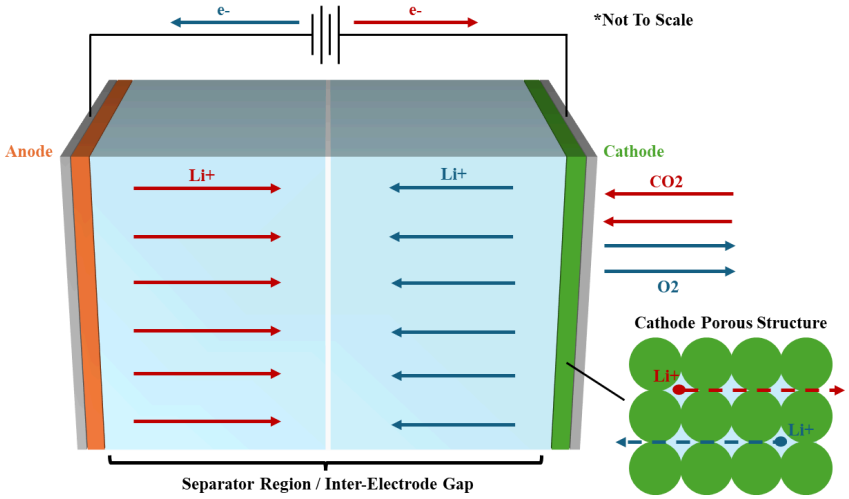

Figure 2: General Cell Structure

AETHER utilizes an electrochemical array to directly recover O_2 from CO_2, with full-scale design discussed in greater detail in Section 1.9. As shown in Figure 2, a single reaction cell consists of a Co-Super P Carbon cathode, a lithium metal anode, and an aprotic LiTFSI/TEGDME electrolyte-immersed separator. The first reaction, represented by Equation 1, oxidizes the anode and draws Li^+ and electrons to the cathode via electrolyte and external wire, respectively. Due to the porosity of the cathode, the Li^+ and electrons contact supplied CO_2, which reduces to the solid product of Li_2CO_3 and C. Equation 2 presents the subsequent lithiation of Li_2CO_3 to Li_2O and C, before Li_2O is oxidized to evolve O_2 as shown in Equation 3 [10]. Thermodynamic potentials (E^0), representative of the minimum voltage required to drive a reaction, are listed as well.

$$3CO_2 + 4Li^+ + 4e^- \rightarrow 2Li_2CO_3 + C \qquad (E^0 = 2.80V) \quad (1)$$

$$Li_2CO_3 + 4Li^+ + 4e^- \rightarrow 3Li_2O + C \qquad (E^0 = 1.43V) \quad (2)$$

$$2Li_2O \rightarrow 4Li^+ + O_2 + 4e^- \qquad (E^0 = 2.91V) \quad (3)$$

AETHER aims to exceed minimum long-duration mission oxygen production requirements; particularly, the system targets a production rate of 4.208 kg O_2 per day for a crew of four astronauts, averaging to 1.052 kg of O_2 per crew member per day (kgO_2/cm-d) [26]. On the ISS, these demands are able to be met by electrolyzing water in the Oxygen Generation Assembly (OGA) due to its desirable location in Low Earth Orbit (LEO) which grants convenient Earth-based resupply; however, extended missions in deep space necessitate near-closed-loop systems [11]. Though some water is generated through the Sabatier reaction, it only produces ~7.5% of the necessary quantity to facilitate operation [11]. As visualized in

Figure 3, the right diagram shows an implementation of AETHER in place of the OGA, which removes the reliance on electrolysis for oxygen production, and thus reduces the necessary water resupply from 1.21 $kgH_2O/cm\text{-}d$ to 0.335 $kgH_2O/cm\text{-}d$. While the AETHER implementation shown does require an increase of O_2 resupply, the overall kg/cm-d of resupply drops 45.5%: from 1.267 kg/cm-d to 0.691 kg/cm-d.

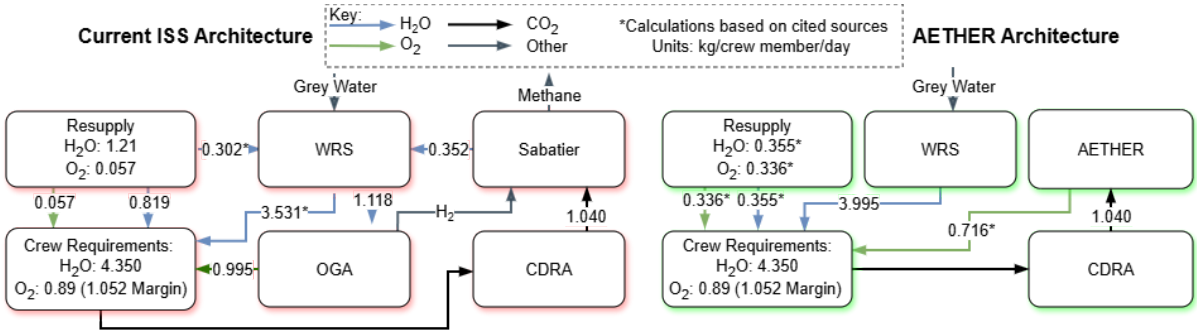

Figure 3: ECLSS With and Without AETHER [11] [12] [13]

The AETHER augmented ECLSS on the right side of Figure 3 lacks electrolysis, leading to the coupling between ECLSS subsystems being greatly reduced. As shown in Figure 3, the OGA relies on the Carbon Dioxide Removal Assembly (CDRA), Sabatier, the Water Recovery System (WRS), and adjacent resupply systems; on the other hand, AETHER relies only on consistent CO_2 supply from the CDRA. Though reducing the number of related subsystems decreases overall system complexity, it also concentrates risk on the remaining subsystems. To mitigate this issue, AETHER will employ a modular design, wherein multiple smaller electrochemical reactions are conducted rather than in one large reactor chamber, as detailed further in section 1.9. Moreover, literature supports the notion that AETHER's electrochemical sequence could operate at comparable efficiencies if exposed to a regular air composition rather than pure CO_2 [10]. Assuming a configuration of 72 cells and at the required oxygen production rate, AETHER at maximum output expects to consume 2084.26 W compared to the OGA's 3573 W. Finally, AETHER cells do not idly draw power, unlike the OGA which draws 382 W while inactive [14].

1.5. Future Advancements

The AETHER system is currently in Phase B of the NASA systems engineering lifecycle, where preliminary design and technology development tests are being carried out [15]. AETHER has reached a Technology Readiness Level (TRL) of 3, as it demonstrates both analytical and experimental proof-of-concept for critical functions and characteristics, including the ability to generate O_2 [16]. By the end of 2027, completion of Phase B and progression to TRL 5 are projected.

As AETHER advances into Phase C the system design will be finalized and tested within simulated operational environments. Following successful validation of oxygen production and system performance, AETHER must establish reliable operation under both microgravity and lunar gravity conditions. Achievement of the stated milestones will allow the system to achieve TRL 6. Additional testing will then be required to ensure that AETHER can produce a consistent and pure O_2 yield capable of sustaining the intended crew size. Once all major validation and environmental testing milestones have been completed, the system will be ready for operational testing in space. TRL 8 will be achieved upon official approval of the full-scale flight-ready system, while TRL 9 will be attained once AETHER successfully operates during an actual spaceflight mission.

1.6. Requirements

In an effort to advance AETHER's TRL, a series of nine requirements were developed based on the HuLC problem statements and requirements to ensure the project is on track with appropriate NASA needs. The critical objectives for AETHER are listed in Table 1 which can be found below. These requirements were derived from the HuLC guidelines and formed the foundation for AETHER's development. AETHER currently meets or is in the process of meeting the requirements listed in Table 1. Additionally, despite only nine requirements being shown in the table, a total of 62 requirements were developed for this project and they can be found in Appendix C, Tables 9 - 11 .

Table 1: AETHER Objective-Derived Critical Requirements

Requirement ID	Requirement Description
CCR-1.0	System shall meet applicable NASA standards.
CCR-1.1	System shall have minimal barriers to NASA adoption.
CCR-1.2	System shall be cost effective with justified estimates.
CCR-1.3	System shall pose no additional risk to the crew.
CCR-1.4	System shall be targeted for operation within the next 5-8 years
CCR-2.2	System shall last the duration of an average lunar mission (30 days).
CCR-2.3	System shall last the duration of an average Mars mission (1200 days).
CCR-3.0	System shall be feasible to operate and implement into NASA Artemis and HLS architectures.
CCR-4.0	System shall improve current ECLSS architectures.

1.7. Verification and Validation

PARSEC has created a list of critical and high-level requirements that will help verify AETHER using the NASA engineering life cycle, (Table 1) [17]. In order to verify requirements per NASA guidelines, PARSEC has laid out a compliance plan for each requirement see Table 2. In Pre-Phase A, project concept studies and a feasibility report were performed to ensure the system could theoretically succeed and be implemented, with emphasis placed on innovation, thereby meeting the requirements CCR 1.0, HRL 10.0 and progressing CCR 1.1, 3.0 and 4.0, see Appendix C. In Phase A, AETHER established a TRL 3, having had the reactions validated in a laboratory environment, research presentations, a proposal and material analysis [10]. In Phase B, AETHER began advancing towards a TRL 4 by building a physical, single-cell, non-cylindrical, scaled-down prototype for experimental validation and performing simulations for full-scale design iterations. To raise the TRL to 4, two primary objectives were decided based on development priorities. The first primary testing objective is to validate the sequentiality of the reactions by cycling through the three voltages consecutively, thus inducing the desired individual reactions separating CO_2 to produce O_2. The second primary objective is to perform a full system test that would validate a cylindrical geometry of AETHER could be feasible. To achieve this, a testing campaign has been established in which a prototype AETHER cell is constructed. The cell will be inserted into a housing that will be positioned within a glove box filled with an inert argon atmosphere. Once the first primary objective has been validated a new synthesis of AETHER will begin for the secondary objective.

Table 2: Critical Requirement Compliance Review

Critical Requirement ID	Compliance Type	Compliance Status	Compliance Plan
CCR-1.0	Analysis	Met	Requirements made in reference to NASA and HuLC guidelines
CCR-1.1	Analysis	In Progress	Integration feasibility analysis
CCR-1.2	Analysis+ Demonstration	Met	Material cost calculation analysis
CCR-1.3	Analysis	In Progress	Hazard and risk assessment done during testing
CCR-1.4	Analysis	Met	Feasibility analysis and system lifespan based on material consumption calculations (timeline)
CCR-2.2	Test	In Progress	System lifespan analysis through testing
CCR-2.3	Test	In Progress	Comparative analysis/system lifespan analysis through testing
CCR-3.0	Demonstrate+Test	In Progress	Demonstrated operability
CCR-4.0	Analysis+ Demonstrait	Met	Full system operation demonstration through simulation

Through analysis, PARSEC evaluated the feasibility and possible effectiveness of AETHER in an effort to create an optimal replacement for the OGS, trade studies and multiple solutions were proposed using mini-proposals based on cost, feasibility, effectiveness, and technical innovation. Assuming a launch cost of $10.8k per kg to lunar orbit insertion, the proposed initial cost calculations save $6.22k per crew member per day in resupply of H_2O and O_2 compared to an OGA implementation justifying the need for a replacement and meets the compliance plan for CCR 1.2 (Table 1). This equates to a cost savings of $4.48m dollars for a 180-day lunar mission with 4 crew members [18].

1.7.1. Simulations

A simulation campaign was conducted using Idaho National Lab's Multiphysics Object-Oriented Simulation Environment (MOOSE). Two models were developed, a macro-scale pseudo-2D (P2D) model to characterize cathode thickness and operational current density, and a micro-scale dendrite growth model to characterize lithium deposits on the anode, which risk puncturing the separator and short-circuiting the cell.

Cell geometry was divided into subdomains of separator and cathode, with the anode represented via a boundary condition. The model solves a system of Partial Differential Equations (PDEs) describing the conservation of charge in the solid phase, conservation of charge in the electrolyte, and conservation of lithium in the electrolyte as listed in Appendix A.3 Equations 7-9. Butler-Volmer kinetics and

overpotential relationships are shown in Appendix A.3 Equation 10-11. Conservation of lithium in the solid phase was neglected due to the lack of intercalation more often seen in lithium-ion cells [19].

Model parameters were selected based on the standard characteristics of similar cells and the LiTFSI/TEGDME electrolyte, including a curve-fit of ionic conductivity as shown in Appendix A.4 Figure 10 [10] [20] [21]. To isolate the effect of cathode thickness, the inter-electrode gap was kept constant at 25 μm, while cathode thicknesses of 25, 50, and 75 μm were tested. With each case, the cell was subjected to current densities of $1{\cdot}10^{-2}$, $2{\cdot}10^{-2}$, $3{\cdot}10^{-2}$, $4{\cdot}10^{-2}$, and $5{\cdot}10^{-2}$ A/cm^2. The initial electrolyte concentration was also set to $1{\cdot}10^{-3}$ mol/cm^3. For converged cases, steady-state voltage and minimum lithium ion concentration were tabulated and compared. Additionally, the Buckingham Pi Theorem was applied to obtain scalability factors. These Π variables are detailed in Appendix A.5 Equations 12-13.

Similar to Figure 4, regions of lowest lithium ion concentration were consistently located near the cathode current collector for all cases. Minimum concentrations held similar magnitudes across similar current densities, regardless of cathode thickness. For instance, cases subjected to $1{\cdot}10^{-2}$ A/cm^2 had minimum concentrations of $8.998{\cdot}10^{-4}$, $9.308{\cdot}10^{-4}$, and $9.406{\cdot}10^{-4}$ mol/cm^3, signifying safe operation but sluggish reaction rates compared to other cases. Appendix A.6 Figure 11 presents a relevant case. Generally, an applied current density that suggests steady reaction but allows for some lithium ion penetration represents a better configuration, such as in Figure 4. However, it should be noted that two cases, pertaining to 50 and 75 μm cathodes under $5{\cdot}10^{-2}$ A/cm^2, diverged. Before diverging, both cases reported full depletion of lithium ions at the back of the cathode and warped electrolyte potential profiles, which indicates a transport limit had been reached. Appendix A.6 Figure 12 presents one of these cases. Overall, stable operation was observed for $\Pi_2 > 0.699$ for all cathode thicknesses and $\Pi_2 < 0.559$ led to divergence for cases of $\Pi_1 > 2$.

Figure 4: P2D-Based Model t = 3600s (50 μm Cathode, $4{\cdot}10^{-2}$ A/cm^2 Case)
(a) Li$^+$ Concentration, (b) Potential In Electrolyte, (c) Potential In Solid Phase

While the Π variables allow for preliminary scaling of the system, several significant assumptions were made that should be noted: (1) lithium electrodeposition was neglected due to the complexity of integrating it with the P2D-based model; (2) reaction rate variation due to evolving porosity, as estimated in Section 1.9, was also not integrated into this simulation.

To complement the P2D-based model, a micro-scale model was configured in MOOSE to explore the extent dendrites pose a risk to the long-term operation of AETHER. The model considers the phase-field variable, which determines whether a region represents electrodeposited lithium or electrolyte; chemical potential, which governs lithium ion transport; and conduction, which incorporates electric field lines [22] [23]. These equations are all listed in Appendix A.7 Equations 14-18. A single case was run on a 300 by 300 μm domain with a -0.45 V overpotential.

Starting conditions are shown in Appendix A.8 Figure 13. At 45 s, as in Appendix A.8 Figure 14, true dendrite formation begins; however, chemical and electric potential profiles remain effectively unchanged.

This provides a baseline for any suggested mitigation strategy, i.e. a suggested strategy can allow minor dendrite formation but must keep potential profiles even. Severe growth can be seen at the 80 s and 115 s timestamps, corresponding to Appendix A.8 Figures 15 and 16, where concentrations in electric potential shift rightward toward dendrite tips and dark blue regions appear in the chemical potential profile indicative of lithium ion starvation. At 125 s, a dendrite spans the entire 300 µm domain, as seen in Figure 5. Assuming a configuration similar to that of the P2D-based model in which the inter-electrode gap was kept a constant 25 µm, the separator would have certainly been punctured.

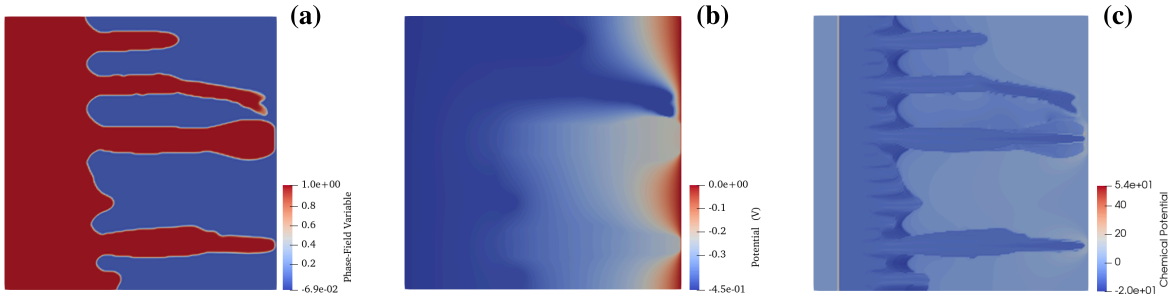

Figure 5: Dendrite Growth Model t = 125s
(a) Phase-Field, (b) Electric Potential, (c) Chemical Potential

The model shows that the primary contributors to exponential dendrite growth are the shifting electric and chemical potentials; therefore, methods that ease transport subsequently reduce dendrite growth. For this reason, induced advective flow may be a valid mitigation strategy to force lithium ions toward the bulk anode surface rather than concentrate at dendrite tip regions. Though sparse, literature supports the notion and claims that there exists a critical Peclet number, a dimensionless variable related to electrolyte flow velocity on the scale of nm/s, at which dendrite formation can be completely alleviated [24]. Advective flow may also allow for greater applied current densities, as lithium ions no longer solely rely on diffusion and migration but rather advection as well. This would modify lithium transport expressions as shown in Appendix A.9 Equations 19-20. Overall, greater applied current densities would lead to greater reaction rates and thus would also improve oxygen production.

1.7.2. Testing Campaign

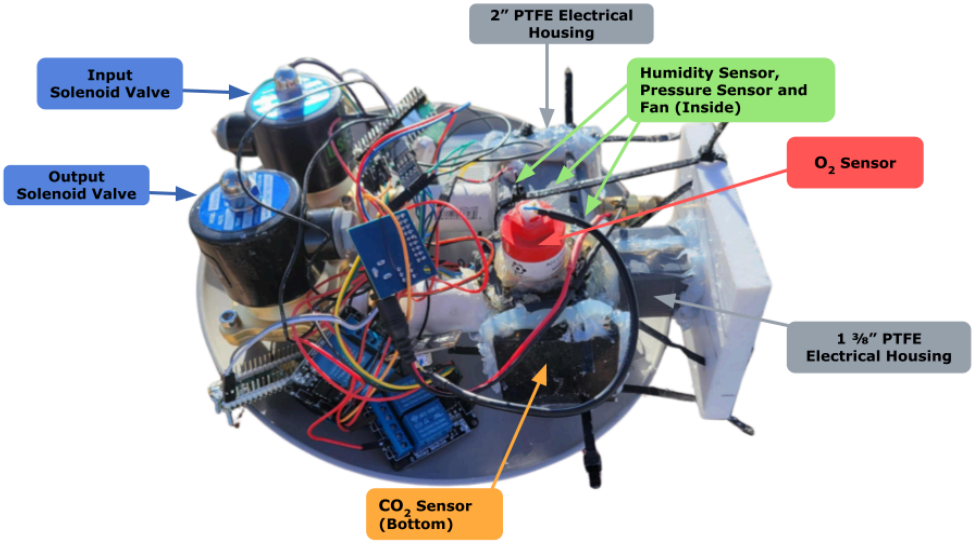

Figure 6: Front View of AETHER Testing Prototype

PARSEC initiated the testing campaign by assembling a testing apparatus that housed AETHER within a 5.35 ft³ argon-filled glovebox. argon is used as an inert mediator to ensure no degradation of the lithium used within AETHER while also allowing for easy measurements of the reactions. The assembly components are enclosed in polyvinyl chloride (PVC) housing with inlet and outlet quick-release hose attachments that allow CO_2 and argon gas to enter the system see Figure 6. Additional internal components include sensors for humidity, pressure, CO_2, and O_2. On the exterior of the glovebox, a pressure release valve is attached to negate the possibility of overpressurization. A potentiostat facilitates the electrochemical reactions needed for operation.

Initial subsystem tests included sensor checks to validate accurate sensor operation. A glove box pressure test was then performed by slowly opening the valve of a high-pressure argon tank connected to the glove box. A spray bottle filled with soapy water was used to check for leaks along the seams. Once sprayed across the seals, if the soapy water bubbled, it indicated a leak. Three found leaks were then marked and documented. Results indicated it took 15 minutes and 300 psi of argon to reach 0% oxygen concentration, which held for approximately 30 minutes inside the glovebox before an increase of oxygen was noted. A dry run of the Planetary Ball Mill (PBM) was also performed, reviewing instructions and safety information accompanying the PBM, including the PBM manual, before running the mill at 100 RPM (noted as 10% of the 1000 RPM capability), with the following cycle: 100 seconds forward (counterclockwise), 20 seconds break, 100 seconds backwards (clockwise) twice [10]. PARSEC placed the Cobalt powder and Co-Super P carbon packages, as well as the PBM pot and lid, spoon, and scale for synthesis inside the glovebox. The glovebox was pressurized before cobalt, carbon, and zirconia balls were sealed within a zirconia milling jar and then subsequently transferred to the PARSEC labspace, ready for PBM insertion. Three forms of synthesis were also performed after subsystem level tests to create the three AETHER disks required for the reactions (1) Cathode Synthesis (2) Lithium Anode Synthesis (3) Electrolyte Separator Synthesis see Appendix D. By producing three physical disks AETHER meets the compliance plan for HRL 7.0, (Table 1). With the preformed synthesis preparations, AETHER still requires Electrolyte Separator Synthesis before performing a full system test with integrated AETHER cells.

1.7.3. Future Testing

To ensure AETHER is viable for space applications, a separate testing campaign will be needed. After the first primary objective is fulfilled, with the conclusion that AETHER can produce O_2 from CO_2 through sequential reactions our critical requirements and compliance plans will have been met meaning the reactions are viable for a prototype. Future tests will be focused on efficiency in a relevant environment and analyzing dendrite formation under load.

1.8. Risks

Full-scale implementation of AETHER presents a series of risks, four being critical with mitigation strategies. Carbon build-up (risk 9) results in eventual degradation of AETHER performance, contaminated out-flow (risk 7) poses a severe airborne particulate hazard to crew, dendrite formation (risk 10) may cause short-circuiting between the anode and cathode, and lithium degradation (risk 5) reduces efficiency of ion reattachment over time. The full breakdown of identified risks can be found in Appendix B, Table 8.

Table 3: AETHER Implementation Risk Matrix

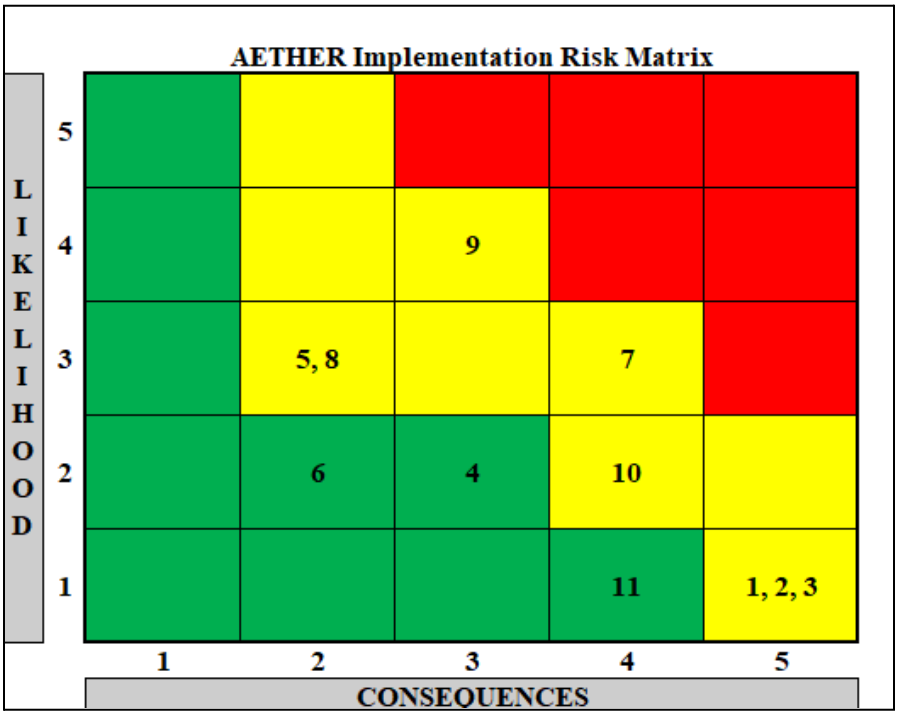

Carbon build-up is the occurrence of excess carbon generated from the reaction depositing on the anode. As the carbon builds up, the exposed surface area of the anode decreases over time, reducing the number of reactions that are able to take place, therefore reducing AETHER's efficiency. Potential methods of counteracting this build-up include employing short reductions of voltage, modifying the composition of the cathode, walnut shell sand-blasting, and supersonic vibrations to physically remove surface-level carbon. Further description of these methods are found in full-scale implementation, below.

Contaminated out-flow of airborne particles would pose a severe physical and health risk to the spacecraft crew or other subsystems. Contamination is likely to contain cobalt, carbon, and polytetrafluoroethylene (PTFE). To mitigate potential contamination, future work must be done to develop filter-like processes to remove stray particulates. These filters may consist of a series of electrostatic, ultrafiltration, or nano filters and would be used as additional layers of safety.

Dendrite formation occurs when a lack of flow exists within the electrolyte, causing ions to unevenly bind and deposit onto the anode. These dendrites have the potential to grow, reducing the quality of the anode's surface and therefore reducing the efficiency of the reaction. Additionally, larger dendrites have the ability to cause the cathode-anode separator to fail, short-circuiting the system. To mitigate this risk, the geometry of the electrolyte layer is to be designed in a specific way to increase the flow of the electrolyte itself, ensuring even distribution of ions.

Lithium degradation is the inherent possibility of the lithium anode degrading over continuous cycles of use, resulting in a decrease in efficiency of ion transfer and potential for increased volatility when exposed with hydrogen. Upon the eventual degradation of the lithium anode, a replacement will be installed to return the system to its full potential.

1.9. Full-Scale Implementation

A cylindrical design was selected for the proposed solution of AETHER due to its maximized reaction surface area along the inside diameter. Utilizing a diffuser, AETHER introduces CO_2 and evenly spreads the gas to the surface of the cathode. After the system is optimally full of CO_2 , the input valves close and the electrochemical reactions start. Upon completion of the reactions, the output valves open to lower pressure. The converted O_2 and all byproducts such as solid carbon particulate flow through a series of filters. Figure 7 shows the input and output processes of AETHER with CO_2 inputs and O_2 outputs.

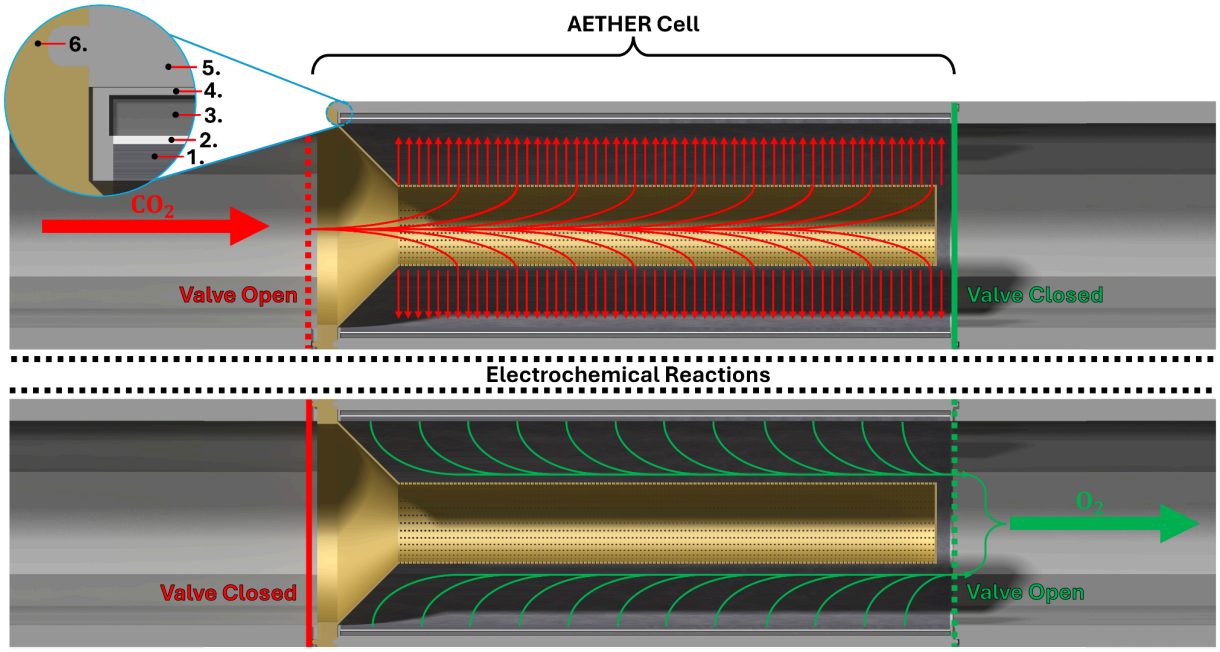

Figure 7: AETHER Cross-section View of Flow

In the upper left of the figure, a detailed view of the layers can be seen. Layer 1 is the cobalt-carbon cathode on which the electrochemical reactions take place (section 1.4). Layer 2 is the glass-fiber separator impregnated with the LiTFSI/TEGDME aprotic electrolyte. Layer 3 is the lithium anode, encased in the same electrolyte to prevent oxidation of the lithium. Including this additional electrolyte layer allows AETHER to operate in a standard atmosphere as opposed to an argon environment. Layer 4 is a non-conductive housing and protective shell made of polyether ether ketone (PEEK). Layer 5 consists of an outer aluminum alloy that interfaces with the diffuser (Layer 6) and connecting inlet and outlet pipes.

As the electrochemical reactions depend on a steady supply of CO_2, the mass transport limitation of the system must be identified. Supporting literature identifies a maximum efficiency of CO_2 gas diffusion electrodes at a current density of 75 mA/cm^2 [25]. Due to this limitation, AETHER's electrochemical reaction is run at a current density of no more than 75 mA/cm^2, although this high current density leads to an increase in dendrite formation rates. To mitigate the formation of dendrites, as mentioned in section 1.7.1, the cross-sectional geometry of the separator is manipulated to induce advective flow. Using an induced advective flow method, a small notched protrusion on the separator is proposed to increase the flow speed of the ions travelling back to the lithium anode at the end of the reactions [26]. Along with the added protrusion to the separator, the lithium anode will have a corresponding slot to encourage faster ion deposition. To further increase this, the lithium anode is separated into multiple anodes radially as shown in Figure 8. Future testing and simulations are required to find the geometry at which dendrite formation

is completely or nearly mitigated, and how many anode divisions would be required to achieve that state. Figure 8 demonstrates the flow streamlines of ions in the electrolyte as they go towards the anode when adjective flow is induced from electrolyte geometry.

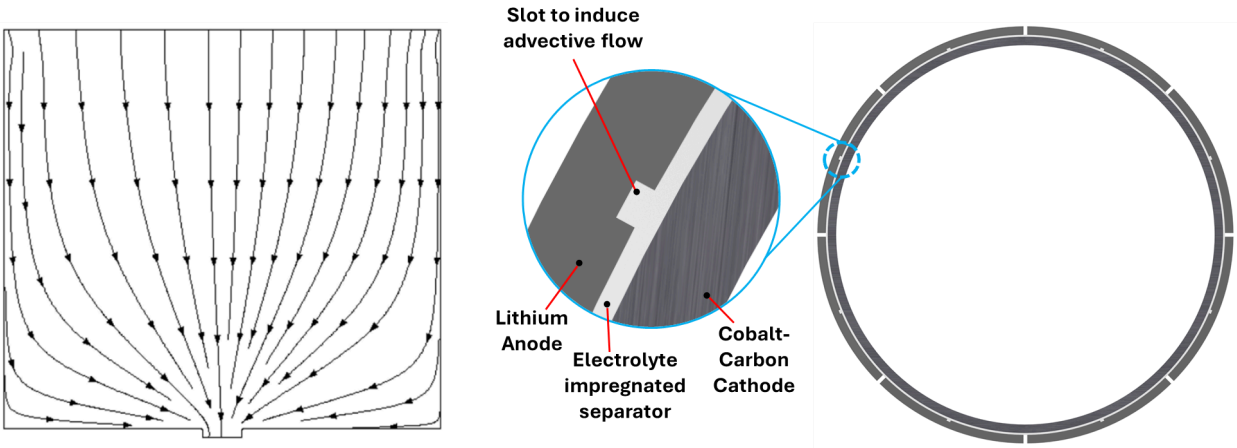

Figure 8: Induced Advective Flow
a) Electrolyte Flow Streamlines [26], b) AETHER Electrode Geometry

In determining how many AETHER cells would be required to sustain a crew, the following assumptions were made: a crew of four members that completes 30 minutes of aerobic exercise and 60 minutes of resistive exercise every day each require 0.89 kg of O_2 and create 1.08 kg of CO_2 daily [27]. Additionally, a margin of 18% was added to the required O_2 for each crew member. Further assumptions include: the efficiency of the electrochemical reactions converting from CO_2 to O_2 is 94.7%, the voltage of the cell for the electrochemical reactions is an average of 2.38 volts, there is 100% faradaic efficiency for O_2 production where four moles of electrons are required to convert one mole of O_2, uniform current density is used to calculate the desired surface area of an assumed non-porous cathode, and no limitations on lifetime such as carbon buildup or dendrite formation occur. *Appendix A. 15, Table 6* shows how for generating oxygen 12 hours a day at a current density of 75.0 mA/cm^2 with a reaction efficiency of 94.7% and a margin of 18% for crew oxygen, a crew of 4 requires 10.5, rounded up to 11, AETHER cells with a cathode inner diameter of 0.1 meters and a length of 0.5 meters and total power of 2.95 kW per day.

Assuming the dendrite formation can be significantly mitigated through induced advective flow, the limiting factor to AETHER cell lifespan is the buildup of carbon as the electrochemical reaction occurs. By using rudimentary stoichiometric and Bruggerman-Percolation simulations, carbon-buildup on the reactive surface of AETHER cells can be estimated. Although these simulations make multiple assumptions about the properties of AETHER that are not yet known, mathematical assumptions are set closer to the worst-case value than the best-case. These simulations also assume that there is zero carbon cleaning ability of the cells.

With an outer cell geometry of 0.5 meters in length and 0.122 meters in diameter, 72 AETHER cells can fit into the size constrained by one ISS Standard Rack (1.05x0.86x2.01m) for simplicity [28]. Assuming an onboard oxygen supply of 0.322 kg/cm-d to make up for the difference of reaction inefficiencies, which was calculated in section 1.4, a 72-cell AETHER system could provide oxygen for a crew of four for 32.83 days before it is unable to meet oxygen demand due to carbon buildup on the reactive surface. This would lead to an AETHER system mass of 641.40 kg, calculated by the mass of one AETHER cell and diffuser being 1.392 kg and 3.381 kg respectively, multiplied by the number of cells, and a 50% mass margin added to account for piping and electronics. The mass also includes the 0.691 kg/cm-d required to

meet crew water and oxygen requirements over a 30 day mission. The modularity of AETHER allows for a wide breadth of configurations to support various mission types, including six-month periods between lunar resupply missions as well as 1200-day Mars missions, as the cells are designed to be easily replaceable. A longer list of mission configuration calculations can be found in *Appendix A. 15, Table 7*. These additional configuration calculations also include theoretical 1200-day Mars missions using AETHER in comparison to the OGA performance. The table shows that for especially long missions, AETHER provides a distinct mass advantage compared to the electrolysis-based OGA. It should be reiterated that this lifespan calculation is assuming zero carbon buildup and mitigation for AETHER.

As AETHER's efficiency and cell lifetime directly depends on the exposed surface area of its cathode, carbon buildup must be mitigated to maximize lifetime. Current research efforts are focused on preventing initial buildup and removing post-formation carbon. Regarding initial mitigation, one approach is the modification of the cathode's chemical components. Incorporating gold and copper into the cathode can improve stability, help maintain high Faradaic efficiency over time, and reduce the overall energy required for the reaction [29]. Another mitigation method utilizes short, periodic reductions in the voltage. This can prevent carbon buildup by periodically clearing the cathode of ions before the cathode can reach the saturation levels that cause solid precipitation [30].

Physical removal of the carbon buildup after its formation is often a more pragmatic approach, as seen implemented in the Series Botch system, which involves taking apart the system and scraping off the carbon buildup by hand [31]. The physical removal of carbon via scraping is not viable as an option in the AETHER system due to the fragility of the cathode, leading to the need of gentler methods of carbon removal. Among these physical removal methods is gentle sandblasting: employing different sand replacements have been adopted to clean delicate surfaces without causing damage. Walnut Blasting, an automotive and aerospace industry-standard method, utilizes finely ground shells as the abrasive medium. However, the spent shell material must be extracted from the reaction chamber via a vacuum system, and the shells themselves degrade upon impact, limiting reuse of the medium to approximately one to two cycles. Walnut shells pose minimal health risks, except in cases of allergy, making them a viable candidate for space-based applications [32].

Alternative methods to physically remove carbon buildup involve utilizing supersonic vibrations. Unlike walnut blasting, vibration-based cleaning is not limited to the external surface area and can effectively address carbon deposition within the porous structure of the cathode. A dry vibrating cleaning cycle could potentially operate concurrently with AETHER's reaction cycles, significantly reducing or eliminating the downtime associated with cleaning cycles. With continuous operation of AETHER, fewer cells are required to produce the required O2, decreasing the system's weight. Other vibration-based cleaning methods include ultrasonic technology, but this would require incorporating injection of a liquid into AETHER's cathode during vibration periods and would involve further research [33].

A finalized AETHER design will likely integrate multiple carbon mitigation methods to achieve an optimized system. As mitigation and cleaning operations for solid carbon buildup continue to develop, the limiting factor of AETHER is expected to shift towards the long-term degradation of the lithium metal anode. If carbon buildup remains a consistent issue, the mass of the lithium anode can be reduced so that it degrades in the same timeframe as the cathode to preserve mass. This approach aligns with AETHER's modular architecture, allowing individual cells to be efficiently removed and replaced.

1.10. Budget

Utilizing NASA's Project Cost Estimating Capability (PCEC) software, an estimate for the cost of implementing AETHER on a long-duration space mission was determined by using First Pound Cost (FPC) Cost Estimating Relationship (CER). The FPC CER produces a cost estimate based on the system's weight (in lb), derived through regression analysis of costs from similar existing systems. The CER provides the raw cost output in FY2015 USD. The given values are then adjusted to FY2028 for the start of Phase C.

The implemented design of AETHER consists of an outermost layer of aluminum piping with a thickness of 5 mm, an inner non-conductive casing made of PEEK with a wall thickness of 0.5 mm, and electrochemical layers consisting of the anode, separator, and cathode with a combined thickness of 1.29 mm. To obtain the required O_2 output for a crew of four over a six-month period, a total of 395 canisters are required, consisting of 72 initial units and 323 replacement units. Each canister measures 303 mm in length with an inner diameter of 122 mm. Based on these design parameters, an initial system mass of 1,137 lb and a replacement parts mass of 992 lb were used in the PCEC. The resulting CER cost output, along with the inflation-adjusted values, are presented in Table 4.

Table 4: PCEC Cost Outputs (Millions of Dollars)

Cost Phase	FY2015 $M	FY2028 $M
Non-Recurring	$223.7	$294.7
Design & Development	$202.8	$267.2
System Test Hardware	$20.9	$27.6
Flight Unit	$16.1	$21.2
Recurring	$16.1	$21.2
Total	**$239.8**	**$315.9**

The non-recurring costs were inflation-adjusted and converted into an annuity distributed across the project life, assuming a 2.6% yearly interest rate. These costs, along with a 50% manufacturing margin and 30% total cost margin, were included in the project's total direct cost. Personnel salaries are also included in the overall cost estimate. Travel costs are omitted with the assumption that personnel live in Huntsville, Alabama and tests will be conducted at NASA's Marshall Space Flight Center. Table 5 provides a breakdown of the current cost estimate for the project, excluding potential changes to launch mission costs.

Table 5: Full Budget Breakdown (Thousands of Dollars)

Mission Phase	Phase C	Phase C	Phase D	Phase D	Phase D	
Year	**FY1 (2028)**	**FY2 (2029)**	**FY3 (2030)**	**FY4 (2031)**	**FY5 (2032)**	**Total ($k)**
PERSONNEL COST						
Science Personnel	80	82	84	86	88	421
Engineering Personnel	320	328	337	345	353	1,683
Technicians	60	62	63	65	66	316
Administration Personnel	120	123	126	129	132	631
Project Management	240	246	252	259	265	1,262
Total Salaries	820	841	863	884	905	4,313
Total ERE	229	235	241	247	253	1,204
Total Personnel	1,049	1,076	1,103	1,131	1,158	5,517
DIRECT COST						
System Cost (from CER)	63,180	64,823	66,465	68,108	69,751	332,327

Manufacturing Margin (50%)	31,590	32,411	33,233	34,054	34,875	166,163
Total Direct Costs	94,770	97,234	99,698	102,162	104,626	498,490
FINAL COST						
Total Projected Cost	95,819	98,310	100,801	103,293	105,784	504,007
Total Cost Margin (30%)	28,746	29,493	30,240	30,988	31,735	151,202
Total Project Cost	124,565	127,803	131,042	134,281	137,519	**655,209**

1.11. Project Timeline

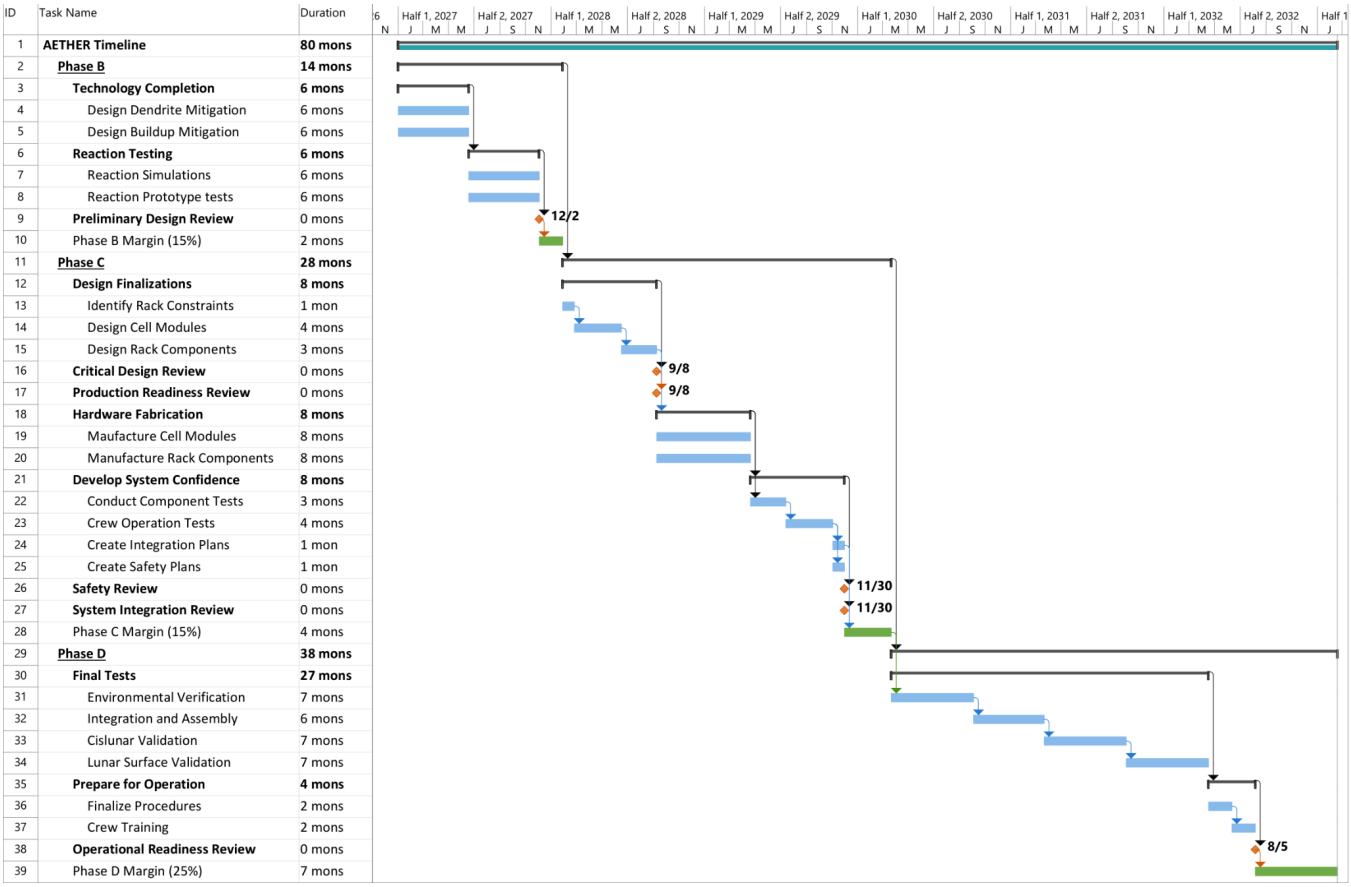

Figure 9: Five-Year Plan Based on NASA's Project Life Cycle (NASA SEH 3.0)

The phases of AETHER's development have been laid out into a 80-month, or a six year and eight month, timeline as seen in Figure 9 with a total included margin of 13 months. Major milestones were based on the NASA Systems Engineering Handbook Project Life Cycle [15]. The blue bars represent major tasks, the orange diamonds represent major review checkpoints, and the green bars represent the time margin built in for each phase of the development.

Phase B focuses on the continued preliminary design and further technology, including tests to verify the preliminary design and simulations to find the operating lifetime. With AETHER's current testing configuration, it is likely that prototype reaction tests and simulations could yield desired results in roughly six months. Phase B will then end with a Preliminary Design Review and achieve a TRL of 5.
Phase C focuses on final design and fabrication of the system given design constraints of a spacecraft of lunar base. Once these constraints are defined, the modular cells and the rest of the AETHER rack

components can be designed. Following the Critical Design and Production Readiness Reviews, cell and rack component manufacturing can begin. Once the components have been produced, further testing can occur to increase the TRL to 6. A Safety and System Integration Review can then be conducted, and AETHER will be ready to integrate into a spacecraft for further testing.

Phase D focuses on the system assembly, integration, and final testing in preparation for full-scale flight tests and operations. System confidence will be ensured through environmental and vibrations testing before orbital and lunar surface tests occur.. Finally, the Operational Readiness Review will be conducted to approve AETHER for use on space missions with crewed operation, achieving a TRL of 8.

1.12. Conclusion

AETHER presents an innovative O_2 reclamation system that utilizes a series of electrochemical reactions to directly recover O_2 from CO_2 with a theoretical efficiency of 97.4% that surpasses current systems. PARSEC's development of AETHER through intensive research, trade studies, and simulation over the past year demonstrate its ability to replace current oxygen reclamation technologies. AETHER's minimal power consumption, low operating temperature, reduced system complexity, modularity, and high reclamation efficiency further establish it for use in long-duration lunar and martian missions.

2. References

[1] Schneider, W., Brown, A., Allen, C., Barta, D., Gazda, D., Mckinley, M., Ridley, A., and Stambaugh, I. *NASA Environmental Control and Life Support Technology Development for Exploration: 2022-2023 Status*. 2023.

[2] National Institute for Aerospace. *2026 Human Lander Challenge Proposal Guidelines*.

[3] Marshall Space Flight Center. *Environmental Control and Life Support System*. 2025.

[4] Barta, D. National Aeronautics and Space Administration Habitation Systems An. *Slidetodoc.com*. https://slidetodoc.com/national-aeronautics-and-space-administration-habitation-systems-an/. Accessed May 28, 2026.

[5] Kim, Y. C. "Exploring Water Production Dynamics in a Sabatier Reactor: A Comprehensive Experimental Investigation." *Fuel*, Vol. 396, 2025, p. 135298. https://doi.org/10.1016/j.fuel.2025.135298.

[6] Crawford, K., Black, C., and Quillen, T. Comprehensive Evaluation of Electrochemical Hydrogen Separator as Hydrogen Recovery Solution for Plasma Pyrolysis Assembly. *Tdl.org*. https://ttu-ir.tdl.org/items/ddcd02e2-fc7d-48b3-a3da-d3a236e6e4d8.

[7] Stanley, C. *Series Bosch Carbon Formation Reactor Trade Study and Down-Select*. 2021.

[8] Abney, M., Mansell, M., Rabenberg, E., Stanley, C., Edmunson, J., Alleman, J., Chen, K., and Dumez, S. "Series-Bosch Technology for Oxygen Recovery during Lunar or Martian Surface Missions." *44th International Conference on Environmental Systems*, 2023.

[9] Abney, M., Mansell, J., Atkins, B., Evans, C., Nur, M., and Beassie, R. "3 Mechanical Designer, Mechanical and Thermal Analysis Branch, Bldg 4877, MSFC, al 35812. 4 Simulation and Analysis, Marshall Space Flight Center, al 35812. 5 NASA Cooperative Student, ECLSS Development Branch, Bldg 4755, MSFC, al 35812. 6 NASA Intern, ECLSS Development Branch." Vol. 115, 2015.

[10] Li, W., Mu, X., Yang, S., Wang, D., Wang, Y., Zhou, H., and He, P. "Artificial Carbon Neutrality through Aprotic CO_2 Splitting." *Angewandte Chemie International Edition*, 2025. https://doi.org/10.1002/anie.202422888.

[11] Ichimura, S., and Yamashiki, Y. A. "Assessment of the Physical and Psychological Aspects of the Current Life Support System on the International Space Station for Sustainable Space Exploration." *Frontiers in Space Technologies*, Vol. 5, 2025. https://doi.org/10.3389/frspt.2024.1461389.

[12] Anderson, M., Ewert, M., and Keener, J. *Life Support Baseline Values and Assumptions Document*. 2018.

[13] Gaskill, M. NASA Achieves Water Recovery Milestone on International Space Station - NASA. *NASA*. https://www.nasa.gov/missions/station/iss-research/nasa-achieves-water-recovery-milestone-on-international-space-station/.

[14] Erickson, R. J., Howe, J., Kulp, G. W., and Van Keuren, S. P. "International Space Station United States Orbital Segment Oxygen Generation System On-Orbit Operational Experience." *SAE International Journal of Aerospace*, Vol. 1, No. 1, 2008, pp. 15–24. https://doi.org/10.4271/2008-01-1962.

[15] NASA. SEH 3.0 NASA Program/Project Life Cycle - NASA. *NASA*. https://www.nasa.gov/reference/3-0-nasa-program-project-life-cycle/.

[16] Manning, C. Technology Readiness Levels. *NASA*. https://www.nasa.gov/directorates/somd/space-communications-navigation-program/technology-readiness-levels/.

[17] NASA. *SYSTEMS ENGINEERING HANDBOOK*.

[18] Jones, H. *Take Material to Space or Make It There?* 2023.

[19] Uddin, K., Perera, S., Widanage, W., Somerville, L., and Marco, J. "Characterising Lithium-Ion Battery Degradation through the Identification and Tracking of Electrochemical Battery Model Parameters." *Batteries*, Vol. 2, No. 2, 2016, p. 13. https://doi.org/10.3390/batteries2020013.

[20] Amangeldi Torayev, Engelke, S., Su, Z., Marbella, L. E., Andrade, V. D., Arnaud Demortière, Pieter C. M. M. Magusin, Merlet, C., Franco, A. A., and Grey, C. P. "Probing and Interpreting the Porosity and Tortuosity Evolution of Li-O_2 Cathodes on Discharge through a Combined Experimental and Theoretical Approach." *The Journal of Physical Chemistry C*, Vol. 125, No. 9, 2021, pp. 4955–4967. https://doi.org/10.1021/acs.jpcc.0c10417.

[21] Chen, J., Chen, C., Huang, T., and Yu, A. "LiTFSI Concentration Optimization in TEGDME Solvent for Lithium–Oxygen Batteries." *ACS Omega*, Vol. 4, No. 24, 2019, pp. 20708–20714. https://doi.org/10.1021/acsomega.9b02941.

[22] Jin, S., Wu, Y., Yang, H., Huang, Y., and Hong, Z. "Protocol for Phase-Field Simulations of Lithium Dendrite Growth with MOOSE Framework." *STAR Protocols*, Vol. 3, No. 4, 2022, p. 101713. https://doi.org/10.1016/j.xpro.2022.101713.

[23] Hong, Z., and Viswanathan, V. “Phase-Field Simulations of Lithium Dendrite Growth with Open-Source Software.” *ACS energy letters*, Vol. 3, No. 7, 2018, pp. 1737–1743. https://doi.org/10.1021/acsenergylett.8b01009.

[24] Parekh, M., and Rahn, C. D. “Flowing Electrolyte Metal Batteries.” *ECS Meeting Abstracts*, Vols. MA2021-01, No. 3, 2021, pp. 233–233. https://doi.org/10.1149/ma2021-013233mtgabs.

[25] Agarwal, V. G., and Haussener, S. “Quantifying Mass Transport Limitations in a Microfluidic CO2 Electrolyzer with a Gas Diffusion Cathode.” *Communications Chemistry*, Vol. 7, No. 1, 2024. https://doi.org/10.1038/s42004-024-01122-5.

[26] Parekh, M. Flowing Electrolyte Metal Batteries - ProQuest. *Proquest.com*. https://www.proquest.com/docview/2652591841?pq-origsite=gscholar&fromopenview=true&sourcetype=Dissertations%20&%20Theses. Accessed May 28, 2026.

[27] Keller, R. J., Porter, W., Goli, K., Rosenthal, R., Butler, N., and Jones, J. A. “Biologically-Based and Physiochemical Life Support and in Situ Resource Utilization for Exploration of the Solar System—Reviewing the Current State and Defining Future Development Needs.” *Life*, Vol. 11, No. 8, 2021, p. 844. https://doi.org/10.3390/life11080844.

[28] Hashimoto, H., Fukatsu, T., Ano, Y., Mizuno, M., and Tokumura, T. Development of International Standard Payload Rack Structure for Space Station Science Operations. *American Institute of Aeronautics and Astronautics*. https://arc.aiaa.org/doi/epdf/10.2514/6.1998-466.

[29] Saprudin, M. H., Jiwanti, P. K., Saprudin, D., Sanjaya, A. R., Putri, Y. M. T. A., Einaga, Y., and Ivandini, T. A. “Electrochemical Reduction of Carbon Dioxide to Acetic Acid on a Cu–Au Modified Boron-Doped Diamond Electrode with a Flow-Cell System.” *RSC Advances*, Vol. 13, No. 32, 2023, pp. 22061–22069. https://doi.org/10.1039/d3ra03836j.

[30] Xu, Y., Edwards, J. P., Liu, S., Rui Kai Miao, Jianan Erick Huang, Gabardo, C. M., O’Brien, C. P., Li, J., and Sargent, E. H. “Self-Cleaning CO_2 Reduction Systems: Unsteady Electrochemical Forcing Enables Stability.” *ACS energy letters*, Vol. 6, No. 2, 2021, pp. 809–815. https://doi.org/10.1021/acsenergylett.0c02401.

[31] Stanley, C., and Moore, E. *Series Bosch Carbon Formation Reactor Trade Study and Down-Select*. 2021.

[32] Kramer, H. Blogs of Kramer Industries. *Kramer Industries Inc*. https://kramerindustriesonline.com/the-benefits-of-walnut-shell-blasting-why-choose-natural-abrasives/. Accessed May 28, 2026.

[33] Hielscher Ultrasonics. The Solution to Electrode Surface Fouling. *Hielscher Ultrasonics*. https://www.hielscher.com/solution-to-electrode-surface-fouling.htm.

Appendix A: Supporting Calculations

A.1 Required Oxygen Production

The required O_2 production rate for a crew of six astronauts per day was determined below, further allowing for the number of required cells and operational current for full-scale implementation of AETHER to be calculated.

$$\dot{m}_{O_2,crew-of-six} = 0.89\,\{kg/day\} \times 6 = 5.34\,\{kg/day\} = 166.88\,\{mol/day\} \quad (1)$$

$$\dot{m}_{O_2,crew-of-six} = 166.88\,\{mol/day\} \times \frac{1\,\{day\}}{86400\,\{s\}} = 1.9315 \times 10^{-3}\ \{mol/s\} \quad (2)$$

A.2 Mass of Implemented AETHER

The assumed weight of the AETHER rack, utilizing an aluminum housing, bronze diffuser and

$$m_{housing} = m_{full\ cell} \times \#\ of\ cells \times 0.5 \quad (3)$$

$$m_{rack} = m_{full\ cell} \times \#\ of\ cells + m_{housing} \quad (4)$$

$$m_{resupply} = m_{replaceable\ parts} \times \#\ of\ required\ replacement\ cells \quad (5)$$

$$m_{total} = m_{rack} + m_{resupply} \quad (6)$$

A.3 P2D-Based Model Equations

The following equations are used for the P2D-based model; in particular, the model considers the conservation of charge in the solid phase, conservation of charge in the electrolyte phase, conservation of lithium in the electrolyte phase, Butler-Volmer kinetics, and overpotential.

$$\nabla \cdot (\sigma_s^{eff} \nabla \phi_s) = a_s j \quad (7)$$

$$\nabla \cdot (\kappa_e^{eff} \nabla \phi_e) + \nabla \cdot (\kappa_{e,D}^{eff} \frac{\nabla c_e}{c_e}) = -a_s j \quad (8)$$

$$\frac{\partial (\varepsilon_e c_e)}{\partial t} = \nabla \cdot (D_e^{eff} \nabla c_e) + \frac{1 - t_+^0}{F} a_s j \quad (9)$$

$$j = k_e (c_e)^{\alpha_a} \left(\exp\left(\frac{\alpha_a F}{RT} \eta \right) - \exp\left(\frac{-\alpha_c F}{RT} \eta \right) \right) \quad (10)$$

$$\eta = \phi_s - \phi_e - U_{ref} \quad (11)$$

A.4 Ionic Conductivity Curve Fit & Expression For LiTFSI/TEGDME Electrolyte

The following figure shows ionic conductivity as a function of LiTFSi concentration, particularly through a fourth-order polynomial.

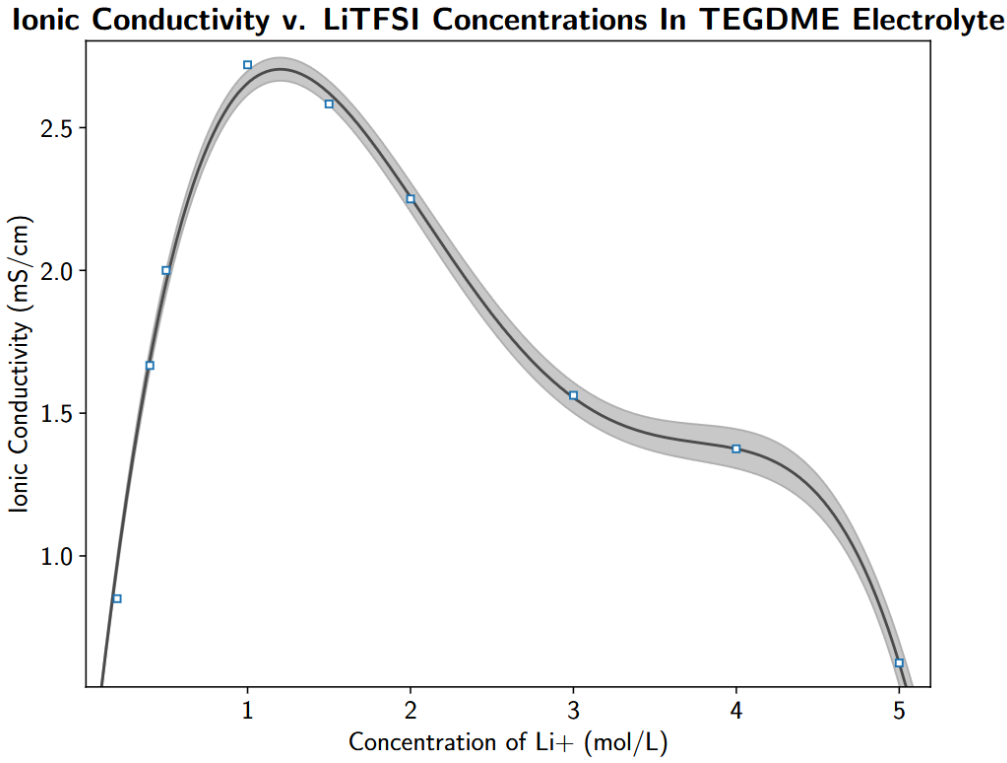

$$\kappa_e = (-8.007 \times 10^{-2})c_e^4 + (9.386 \times 10^{-1})c_e^3 + (-3.782)c_e^2 + (5.579)c_e$$

Figure 10

A.5 Buckingham Pi Variables

The following are dimensionless Π variables derived for the purpose of characterizing simulated cell configurations, particularly for the P2D-based model.

$$\Pi_1 = \frac{t_c}{t_s} \tag{12}$$

$$\Pi_2 = \frac{F c_{e,0} D_e}{t_s j} \tag{13}$$

A.6 P2D-Based Model Plots

The following are contour plots from three cases run with the P2D-based model.

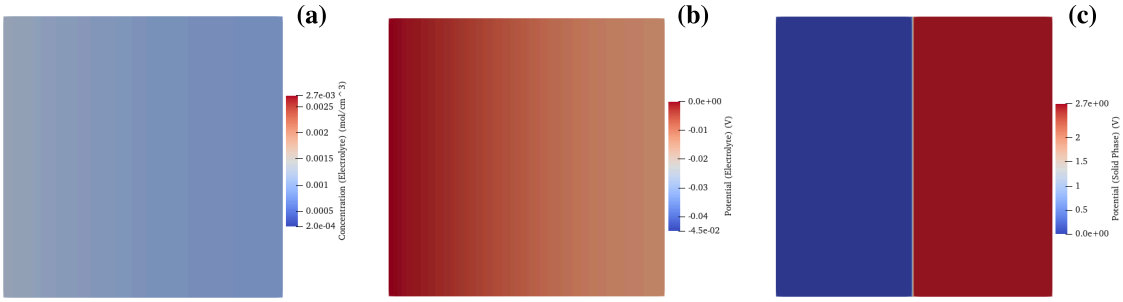

Figure 11: P2D-Based Model t = 3600s (25 µm Cathode, 1·10^{-2} A/cm^2 Case)
(a) Li$^+$ Concentration, (b) Potential In Electrolyte, (c) Potential In Solid Phase

Figure 4: P2D-Based Model t = 3600s (50 µm Cathode, 4·10^{-2} A/cm^2 Case)
(a) Li$^+$ Concentration, (b) Potential In Electrolyte, (c) Potential In Solid Phase

Figure 12: P2D-Based Model t = 27s (75 µm Cathode, 5·10^{-2} A/cm^2 Case)
(a) Li$^+$ Concentration, (b) Potential In Electrolyte, (c) Potential In Solid Phase

A.7 Dendrite Growth Model Equations

The following equations describe dendrite growth and propagation through the phase-field variable, which determines whether a region represents electrodeposited lithium or electrolyte; chemical potential, which governs the transport of lithium ions; and conduction, which incorporates electric field lines.

$$\frac{\partial \xi}{\partial t} = -L_o\left(g'(\xi) - k\nabla^2\xi\right) - L_\eta h'(\xi)\left\{\exp\left[\frac{(1-\alpha)nF\eta_a}{RT}\right] - \frac{c_{Li^+}}{c_0}\exp\left[\frac{-\alpha nF\eta_\alpha}{RT}\right]\right\} \tag{14}$$

$$c_{Li^+} = c^l(1-h(\xi)) = \frac{\exp\left[\frac{(\mu-\varepsilon^l)}{RT}\right]}{1+\exp\left[\frac{(\mu-\varepsilon^l)}{RT}\right]}(1-h(\xi)) \tag{15}$$

$$\chi \frac{\partial \mu}{\partial t} = \nabla \cdot \frac{D c_{Li^+}}{RT} [\nabla \mu + nF \nabla \phi] - \frac{\partial h(\xi)}{\partial t} \left[c^s \frac{C_m^s}{C_m^l} - c^l \right] \tag{16}$$

$$\chi = \frac{\partial c^l}{\partial \mu} [1 - h(\xi)] + \frac{\partial c^s}{\partial \mu} h(\xi) \frac{C_m^s}{C_m^l} \tag{17}$$

$$\nabla \sigma \nabla \phi = nF C_m^s \frac{\partial \xi}{\partial t} \tag{18}$$

A.8 Dendrite Growth Model Plots

The following are contour plots of the same dendrite growth simulation at different timestamps.

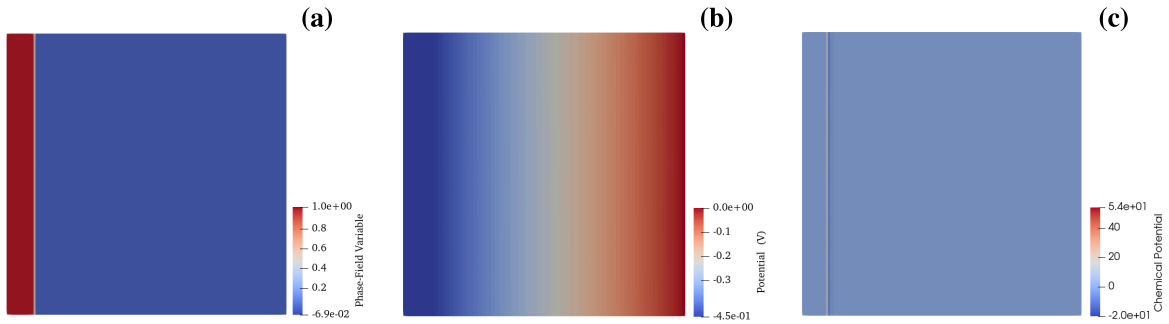

Figure 13: Dendrite Growth Model t = 0s
(a) Phase-Field, (b) Electric Potential, (c) Chemical Potential

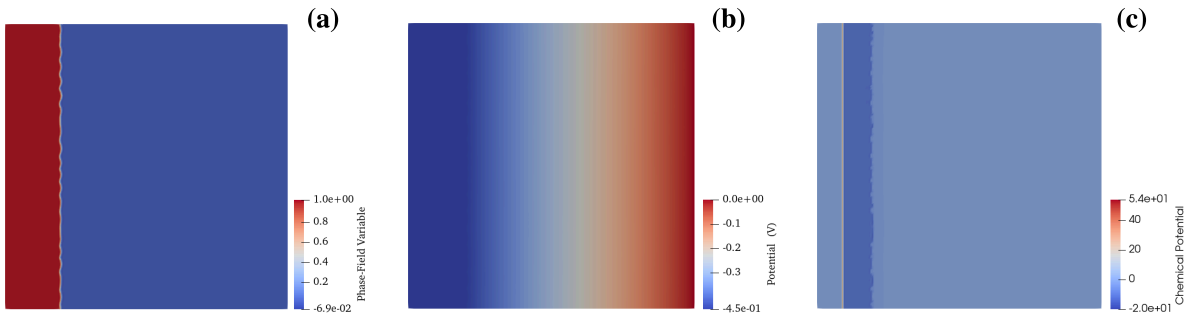

Figure 14: Dendrite Growth Model t = 45s
(a) Phase-Field, (b) Electric Potential, (c) Chemical Potential

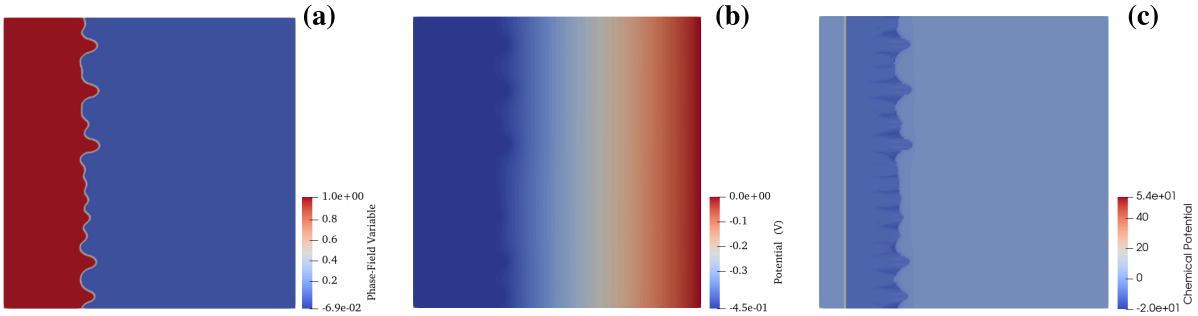

Figure 15: Dendrite Growth Model t = 80s
(a) Phase-Field, (b) Electric Potential, (c) Chemical Potential

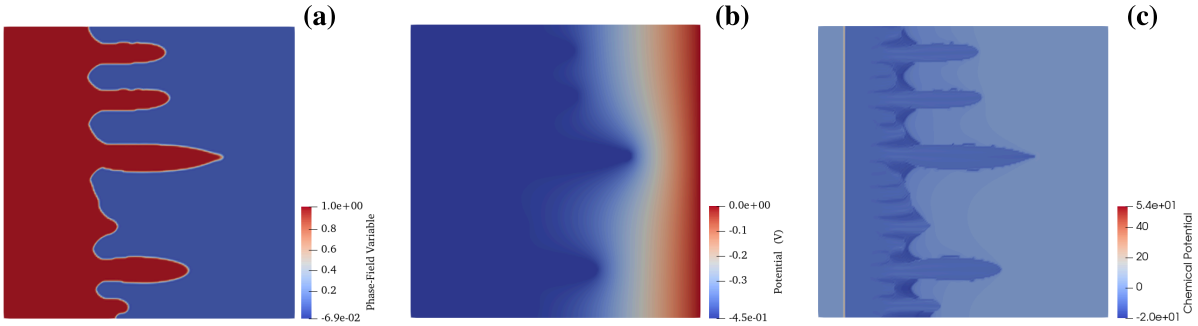

Figure 16: Dendrite Growth Model t = 115s
(a) Phase-Field, (b) Electric Potential, (c) Chemical Potential

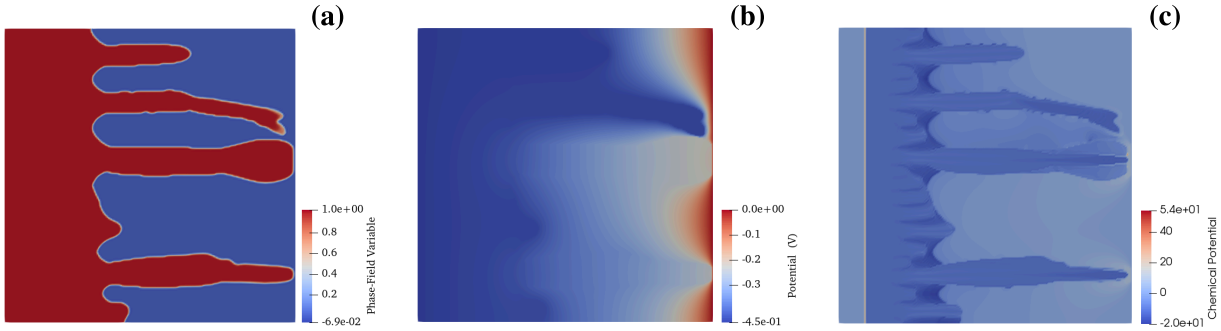

Figure 5: Dendrite Growth Model t = 125s
(a) Phase-Field, (b) Electric Potential, (c) Chemical Potential

A.9 Electrolyte Phase Li^+ Transport Variations

Governing equations describing the conservation of lithium in the electrolyte phase; specifically, the first form represents the standard variation and the second form incorporates an advective flow term.

$$\frac{\partial(\varepsilon_e c_e)}{\partial t} = \nabla \cdot (D_e^{eff} \nabla c_e) + \frac{1 - t_+^0}{F} a_s j \tag{19}$$

$$\frac{\partial(\varepsilon_e c_e)}{\partial t} = \nabla \cdot (D_e^{eff} \nabla c_e) + \frac{1 - t_+^0}{F} a_s j + \mathbf{b} \cdot \nabla c_e \tag{20}$$

A.10 AETHER Required Number of Cells for a Crew of Four per day

Given a cathode inner diameter of 0.1 meters and a length of 0.5 meters, the following results were calculated using current density, number of crew, and O_2 required per crew member per day as inputs.

Table 6: Required Number of Cells Code Output

Runtime (hrs)	Current Density (A/m^2)	Cathode Surface Area (m^2)	Number of Cells	Power (Watts)
8.00	500.00	3.72	23.65	4421.31
8.00	550.00	3.38	21.50	4421.31
8.00	600.00	3.10	19.71	4421.31
8.00	650.00	2.86	18.19	4421.31
8.00	700.00	2.65	16.89	4421.31
8.00	750.00	2.48	15.77	4421.31
12.00	500.00	2.48	15.77	2947.54
12.00	550.00	2.25	14.34	2947.54
12.00	600.00	2.06	13.14	2947.54
12.00	650.00	1.91	12.13	2947.54
12.00	700.00	1.77	11.26	2947.54
12.00	750.00	1.65	10.51	2947.54
18.00	500.00	1.65	10.51	1965.03
18.00	550.00	1.50	9.56	1965.03

18.00	600.00	1.38	8.76	1965.03
18.00	650.00	1.27	8.09	1965.03
18.00	700.00	1.18	7.51	1965.03
18.00	750.00	1.10	7.01	1965.03

Table 7: AETHER Cell Configuration Comparisons For Four Crew

Mission Length (Days)	Cells (Replacements to Mission Length)	Cells Lifetime (Days)	Total Mass Including Supply To Sustain Crew (kg)	Estimated Total Mass Including Supply To Sustain Crew with OGA (kg)	Avg. Power per Cells Lifetime (Watts)
30	43 (23)	19.60	578.52	874.57	1233.24
30	72 (0)	32.83	754.40	874.57	2084.26
180	43 (352)	19.60	1451.10	1924.87	1233.24
180	72 (323)	32.83	1618.23	1924.87	2084.26
1200	72 (2560)	32.83	7551.07	9066.91	2084.26
1200	144 (2489)	65.65	7967.49	9066.91	4199.32

Appendix B: Risk Table

Table 8: AETHER Implementation Risks

ID	Risk Name	Description	Related Systems	L	C	Method	Plan
1	Cobalt Spontaneous Combustion	Cobalt may spontaneously ignite due to its pyrophoric nature, or due to shock, vibrations, or friction, potentially harming system functionality and or crewmembers.	Cathode, Reactants	1	5	M	Electrostatic, ultrafine, and nanoparticle filters will be employed to deny the possibility of uncontrolled cobalt powder exposure to a spacecraft environment.

2	Lithium Oxygenation	Lithium can violently combust when exposed to oxygen, potentially causing damage to personnel, testing materials, and the environment.	Cathode, Reactants	1	5	M	Lithium will only be handled while under an inert argon atmosphere, and will be stored in an airtight container with an argon atmosphere.
3	Lithium Hydrogenation	Lithium can violently combust when exposed to water and other hydrogen ions, potentially causing damage to personnel, testing materials, and the environment.	Anode, Reactants	1	5	M	Lithium will only be handled while under an inert argon atmosphere, and will be stored in an airtight container with an argon atmosphere.
4	Cathode/Anode Failure	Improper ionization separators can compromise the capability of the system to reclaim carbon dioxide.	Cathode, Anode	2	3	M	By employing multiple cathode/anode modules a loss of one module can be mitigated. Following a singular module failure the crew must replace the failed module.
5	Lithium Degradation	Lithium has the potential to degrade over time when in contact with the atmosphere, decreasing efficiency in ion transfer as well as increasing volatility when exposed to hydrogen.	Anode, Reactants	3	2	A	Upon eventual degradation of Lithium anode, a replacement must be installed, ensuring proper disposal procedures in a

							humidity free environment.
6	Humidity Exposure	System exposure to humidity can degrade the cathode and anode leading to a loss in efficiency.	Cathode, Anode, Filtration	2	2	M	Filtration system will employ adequate humidity reduction filters and must be replaced following buildup leading to increase in humidity in the system. Any degraded Anodes or Cathodes should be promptly replaced by the crew.
7	Contaminated Out-flow	AETHER out-flow can be contaminated with Carbon, Cobalt, or PTFE dust which may pose a severe health and safety risk to crewmembers.	Filtration	3	4	M	A series of electrostatic, ultrafiltration and nanofilters will be employed to ensure no contaminants exist in AETHER's out flow. If such filters fail proper cleaning or replacement procedures must be conducted to ensure a restoration to full system functionality.
8	Particulate Buildup	AETHER in-flow may contain	Filtration	3	2	M	Nanoscale and Electrostatic

		particulates, which can build-up on the surface of the cathode, leading to a loss in reaction efficiency					filters will be employed to ensure no particulates enter the AETHER reaction chamber. If such filters fail, proper cleaning or replacement procedures must be conducted to ensure a restoration to full system functionality.
9	Carbon Buildup	Carbon extracted from CO_2 may deposit onto the cathode, reducing the efficiency of AETHER with a replacement module being required if the buildup hits a criticality point.	Filtration, Cathode, Reactants	4	3	M	Potential methods of mitigation include using walnut shell sand-blasting and supersonic vibrations to remove surface-level carbon.
10	Dendrite Formation	Lithium dendrites may occur along the surface of the anode, reducing the quality of the surface of the anode, thus reducing the reaction effectiveness. Large dendrites have the potential to cause the cathode-anode separator to fail.	Cathode, Reactants	2	4	M	Specialized geometry will be employed to ensure ions are able to move fast enough to reattach to the anode uniformly.
11	Electrical Failure	Loss of connectivity between the power source and the cathode/anode can	Circuitry, Power, Cathode, Anode	1	4	M	Ensure all AETHER modules are wired in

		lead to a decrease in system efficiency. Failure of the power source to deliver proper potential difference to the cathode/anode can lead to a decrease in efficiency					parallel as well as redundant power sources. If any connection fails, the crew must follow proper repair procedures to ensure restoration to full system functionality.

Appendix C: Requirements

Table 9: Challenge Critical Requirements

Req #	Requirement	Rationale	Parent Req.	Child Req.	Verification Method
CCR-1-0	System shall meet NASA standards	HuLC Guidelines		CCR-1-1,1-2,1-3	Analysis
CCR-1-1	System shall have minimal barriers to NASA adoption	HuLC Guidelines	CCR-1-0		Analysis
CCR-1-2	System shall be cost effective with justified estimates	HuLC Guidelines	CCR-1-0		Analysis
CCR-1-3	System shall pose no additional risk to the crew	HuLC Guidelines	CCR-1-0	HLR-4-0	Analysis
CCR-1-4	System shall be targeted for operational use within 5-8 years	HuLC Guidelines	CCR-1-0		Analysis
CCR-2-0	System shall withstand operational environments	HuLC Guidelines		CCR-2-1, 2-2, 2-3, 2-4, 2-5, HLR-1-0, 2-0, 8-0	Analysis

CCR-2-1	System shall withstand Launch Loads	HuLC Guidelines	CCR-2-0		Analysis
CCR-2-2	System shall last the duration of an average Lunar Mission - 30 Days	HuLC Guidelines	CCR-2-0		Analysis
CCR-2-3	System shall last the duration of an average Martian mission - 1200 Days	HuLC Guidelines	CCR-2-0		Analysis
CCR-2-4	System shall be able to withstand radiation exposure	HuLC Guidelines	CCR-2-0		Analysis
CCR-2-5	System shall be able to withstand the vacuum environment	HuLC Guidelines	CCR-2-0		Analysis
CCR-3-0	System shall be simple to implement, operate and understand	HuLC Guidelines		HLR-6-0	Inspection
CCR-4-0	System shall be capable of improving current NASA ECLSS systems	HuLC Guidelines		HLR-3-0, 5-0, 7-0, 9-0	Test

Table 10: High Level Requirements

Req #	Requirement	Rationale	Parent Req.	Child Req.	Verification Method
HLR-1-0	System shall be able to withstand Lunar Regolith	To allow for operation in a regolith environment	CCR-2-0	LLR-1-0,1-1	Analysis
HLR-2-0	System shall be able to withstand Martian Regolith	To allow for operation in a regolith environment	CCR-2-0	LLR-1-0,1-1	Analysis
HLR-3-0	System shall yield >50% oxygen reclamation for the duration of a mission	System functionality	CCR-4-0	HLR-3-1, LLR-14-0,15-0, 16-0	Analysis
HLR-3-1	System shall be capable of providing O_2 to 6 astronauts per day	System functionality	HLR-3-0	LLR-14-0	Analysis/Demonstration
HLR-4-0	System shall be hydrated with a non-aqueous based solution	To ensure safety to the crew by mitigating the risk of explosion or fire	CCR-1-3	HLR-4-1, 4-2, 4-3	Inspection
HLR-4-1	System shall be kept in an airtight container	To ensure safety to the crew by mitigating the risk of explosion or fire	HLR-4-0	LLR-17-0, 17-1	Inspection

HLR-4-2	System shall be kept in a watertight container	To ensure safety to the crew by mitigating the risk of explosion or fire	HLR-4-0		Inspection
HLR-4-3	System's chemical reactions and reactants shall be kept independent from the crew compartments	To ensure safety to the crew by mitigating the risk of explosion, fire, and exposure to carcinogenic	HLR-4-0	LLR-2-0,2-1,10-0,11-0	Inspection
HLR-5-0	System shall not use more than 86 kWh	System functionality	CCR-4-0	HLR-5-1, LLR-12-0	Test
HLR-5-1	System shall be electronically grounded	System functionality	HLR-5-0	LLR-12-0	Inspection
HLR-6-0	Systems' replaceable components must be accessible	System functionality	CCR-3-0	LLR-2-0,2-1,3-0,4-0	Demonstration
HLR-7-0	System shall have 3 disks forming an electrolyzer cell	System functionality	CCR-4-0	LLR-5-0,6-0,6-1,6-2,6-3,6-4,6-5,6-6, 7-0,7-1,7-2,8-0,8-1,8-2,8-3	Test
HLR-8-0	System shall have below 2% interior aqueous-based humidity	To ensure safety to the crew by mitigating the risk of explosion or fire	CCR-2-0	LLR-9-0, 13-0	Test

HLR-9-0	Weights requirements (When research is done)	HuLC Guidelines	CCR-4-0		Inspection
HLR-10-0	System shall be scalable	Integration into HLS/Gateway	CCR-3-0, 4-0		Analysis
HLR-11-0	System shall be able to accommodate entire AETHER reaction in one cycle	System functionality	CCR-3-0		Test

Table 11: Low Level Requirements

Req #	Requirement	Rationale	Parent Req.	Child Req.	Verification Method
LLR-1-0	System input shall only be pure CO_2	System functionality	HLR 1-0, 2-0	LLR-1-1	Test
LLR-1-1	System shall allow for an input of varying amounts of CO_2	System functionality	LLR-1-0		Analysis
LLR-2-0	Removable parts shall be done in a closed environment.	System functionality	HLR 4-3, 6-0	LLR-2-1	Analysis
LLR-2-1	Disks shall be kept in a closed environment to prevent contamination	System functionality	LLR-2-0		Analysis
LLR-3-0	System's plates shall be externally accessible for replacement	Ease of system functionality	HLR-6-0		Analysis

LLR-4-0	System's filters shall be externally accessible for replacement	Ease of system functionality	HLR 6-0		Analysis
LLR-5-0	System's aprotic electrolyte will be housed in a GF/A membrane	System functionality	HRL-7-0		Inspection
LLR-6-0	System shall utilize a cobalt disk	System functionality	HLR-7-0	LLR-6-1, 6-2, 6-3, 6-4, 6-5, 6-6	Inspection
LLR-6-1	System shall have a Cathode plate no larger than 2.4cm +-0.01 in diameter	System functionality	LLR-6-0		Inspection
LLR-6-2	System shall be capable of providing a voltage equal to or less than 2.8 V to the Cobalt plate	System functionality	LLR-6-0		Test
LLR-6-3	System shall be capable of providing a voltage equal to or less than 1.43 V to the Cobalt plate	System functionality	LLR-6-0		Test
LLR-6-4	System's Cobalt disk shall be comprised of Co-Super P Carbon with a PTFE binder	System functionality	LLR-6-0		Test

LLR-6-5	System's Cobalt disk shall have a maximal porous surface area	System functionality	LLR-6-0		Analysis
LLR-6-6	System shall use the electrolytes and the PTFE binder to hydrate the cobalt	System functionality	LLR-6-0		Test
LLR-7-0	System shall utilize a separating disk	System functionality	HLR-7-0	LLR-7-1, 7-2, 7-2	Test
LLR-7-1	System's aprotic electrolyte membrane (AEM) shall be a 2.75cm +- 0.01 diameter	System functionality	LLR-7-0		Inspection
LLR-7-2	System's separating disk shall be comprised of the AEM	System functionality	LLR-7-0		Inspection
LLR-7-3	System's separating disk membrane shall be PE, GF/A, or cellulose	System functionality	LLR-7-0		Inspection
LLR-8-0	System shall utilize a lithium disk	System functionality	HLR-7-0	LLR-8-1, 8-2, 8-3	Test
LLR-8-1	System shall have an Anode plate no larger than 2.4cm +-0.01 in diameter	System functionality	LLR-8-0		Inspection

LLR-8-2	System shall be capable of producing a voltage greater than 2.91 V to the Lithium plate	System functionality	LLR-8-0		Test
LLR-8-3	System's anode disk shall be a Lithium Foil Anode	System functionality	LLR-8-0		Inspection
LLR-9-0	System shall be capable of detecting real humidity within the 2% requirement	System functionality	HLR 8-0		Analysis
LLR-10-0	System shall be operated in an inert argon environment	To ensure safety to the crew by mitigating the risk of explosion or fire	HLR 4-3		Analysis
LLR-11-0	System shall be assembled in an inert argon environment	To ensure safety to the crew by mitigating the risk of explosion or fire	HLR 4-3		Analysis
LLR-12-0	System shall have a potentiostat and galvanostat connecting the cathode and anode	System functionality	HLR-5-0, HRL-5-1		Inspection
LLR-13-0	System shall detect temperature +-5f degrees of accuracy	System functionality	HLR-8-0		Analysis

LLR-14-0	System shall detect O_2 in the sensing area with +-1% accuracy	System functionality	HLR-3-0, HLR-3-1		Analysis
LLR-15-0	System shall detect all CO_2 in the sensing area with +-1% accuracy	System functionality	HLR-3-0		Analysis
LLR-16-0	System shall yield > 50% oxygen reclamation for the duration of the testing phase	System functionality	HLR-3-0		Test
LLR-17-0	System shall have an internal pressure of TBR bar	System functionality	HLR-4-1	LLR-17-1	Test
LLR-17-1	The system shall not have an internal pressure higher than the atmospheric pressure	To ensure safety to the crew by mitigating the risk of explosion or fire	LLR-17-0		Test
LLR-18-0	System shall measure the input and output of the system	System functionality	HLR-3-0		Test

Appendix D: Testing

Table 12: AETHER Existing Test Status & Results

Test	Objective	Status	Results
Power & Electronics Integration Test	Verify accurate power distribution and sensor readings via bluetooth.	Successful	Sensors operated and provided correct readings.
Glovebox argon	Verify glove box	Successful	Ensured minimal

Pressurization Test	integrity measures O_2, humidity, concentration, CO_2 pressure.		leaks from argon Glovebox and ensured functional sensors.
Planetary Ball Mill Cathode Synthesis	Form the porous Co-Super P cathode utilizing a Planetary Ball Mill.	Successful	Porous Co-Super P cathode successfully formed.
Lithium Anode Synthesis	Form the Lithium anode.	Successful	Lithium anode disks formed in argon environment.
Electrolyte Separator Synthesis	Form the LiTFSI /TEGDME Aprotic Electrolyte Separator.	Not Completed	Not yet conducted.
AETHER Final Testing	Integrated test of the cathode, anode and separator to verify the electrochemical reaction.	Not Completed	Not yet conducted.